Tumor-derived PD-L1 + exosomes with natural inflammation tropism for psoriasis-targeted treatment

Honglin Jia
Third Military of Medical University
Tao Liu
Third Military of Medical University
Qunfang Yang
Third Military of Medical University
Haiping zheng
Xiamen University
Shixiang Fu
The NCO School of Army Medical University
Jiahui Hong
Third Military of Medical University
Zechen Zhou
Third Military of Medical University
Haigang Zhang
Third Military of Medical University
Xiaohong Chen
Third Military of Medical University
RenShan Sun
Shenzhen University
Wenjun Shan (wjshan@tmmu.edu.cn)
Third Military of Medical University

Research Article

Keywords: Psoriasis, Exosomes, Pristimerin, PD-L1, Ferroptosis

Posted Date: August 9th, 2022

DOI: https://doi.org/10.21203/rs.3.rs-1901103/v1

Abstract

Background: Psoriasis is a chronic and readily recurrent inflammatory skin disease. To date, there is no cure for psoriasis and significant challenges remain in developing more safe and efficacious novel targeted therapies. Psoriasis is characterized by abnormal activation of the immune system, and hyperproliferation and aberrant differentiation of keratinocytes. Psoriatic keratinocytes death is also recently recognized as a major amplifier to the initiation of inflammatory cascade. Given that both keratinocytes and immune cells express high PD-1 in psoriasis, which imply PD-1 as a potential therapeutic target for psoriasis. Here, we developed a well-structured pristimerin nanodot-loaded PD-L1 positive exosome derived from tumor cells (Pri@exo) and elucidated their targeting therapeutic effects.

Results: The Pri@exo displays strong cellular uptake and intracellular retention in active $CD4^+$ T cells and HaCaT keratinocytes, suggesting the PD-1^+ cells targeting capacity of Pri@exo. Remarkably, Pri@exo significantly and safely reversed imiquimod (IMQ)-induced psoriasis in mice, indicated by reducing epidermal thickness, decreasing plaque formation, and over-activating inflammation since it targeted both $CD4^+$ T cells and keratinocytes gathering around the lesion. The increasing inflammatory cytokine excretion of $CD4^+$ T cells in psoriasis was suppressed by Pri@exo. Besides, Pri@exo treatment alleviated ferroptosis-related changes in psoriatic skin, thereby dampening excessive inflammation and, in turn, decreasing the abnormal proliferation of keratinocytes in psoriatic lesions.

Conclusion: This tumor-derived PD-$L1^+$ exosomes has a natural inflammatory tropism and excellent anti-inflammatory effect, and able to act as a bio-inspired nanocarrier for various therapeutic agents to optimized inflammatory disease therapy.

Introduction

With their increasing prevalence, inflammatory skin diseases are becoming a major public health concern. Psoriasis, an inflammatory skin disease, is one of the most persistent diseases characterized by the activation of innate and adaptive immune responses, often through the production of proinflammatory cytokines[1, 2]. The pathogenesis of psoriasis is generally contemplated as an aberrant activation of dendritic cells and T cell-mediated autoimmune responses with complex cellular networks[2]. Currently, the treatment options available to patients with psoriasis are limited[3]. Although topical glucocorticoids and immunosuppressants remain the first-line treatment options, most patients do not respond well to topical or systemic glucocorticoid therapy, especially long-term therapy, owing to glucocorticoid resistance and off-target effects[1, 4, 5]. Exploring a targeted therapy strategy is urgent for improving psoriasis treatment.

Various nanocarriers are currently designed for drug loading and delivery to inflammatory sites with higher targeting and lower toxic effects[3, 6]. However, nanoparticle-based drug delivery systems still possess some inherent disadvantages, such as the immunogenicity and toxicity of the carrier itself, rapid

immune recognition and blood clearance, and poor biodistribution[3]. Therefore, developing more reliable and effective treatment options for psoriasis is highly desirable but challenging.

Recently, considerable progress has been made in the field of exosomes, which is a kind of nanovesicle (30–150 nm) secreted by various cell types with unique natural properties, including excellent biocompatibility, low cellularity toxicity and immunogenicity, and target specificity[7]. Exosomes derived from tumor cells, immune cells, and mesenchymal stem cells have been successfully applied to encapsulate and deliver chemotherapeutic drugs, nucleic acid drugs, neurotransmitters, and even nanoparticles to treat various diseases such as cancer and neurological diseases[7, 8]. However, it has rarely been reported to treat inflammatory skin diseases. It is particularly noteworthy that in addition to their unique properties, exosomes enrich specific contents (such as RNA, DNA, proteins, and small molecules) derived from parental cells, thereby engrafting the natural biological functions of primitive cells, and can even be used directly for disease treatment[7, 8]. Recent studies have found that tumor cells such as melanoma secrete high levels of programmed death-ligand 1 (PD-L1) on exosomes to achieve immune escape[9, 10]. The PD-L1$^+$ exosomes can reach the draining lymph nodes and suppress T cell activity in an immunosuppressive manner, implying that the tumor-derived exosomes have potential inflammatory tropism and anti-inflammatory therapeutic effects[9].

In this study, we chose melanoma cell-derived exosomes for targeted delivery of pristimerin, a naturally occurring triterpenoid biologically active chemical exhibiting an anti-inflammatory effect, to cells overactive in the inflammatory process of psoriasis via PD-1/PD-L1 interaction[11]. We yielded well-structured pristimerin nanodot-loaded exosomes (Pri@exo) and elucidated their targeting and therapeutic effects on activated CD4$^+$ T cells and keratinocytes. To improve Pri@exo sustained-release properties on the skin, we introduced Pluronic F127 thermosensitive hydrogel and evaluated its biodistribution *in vivo*. We confirmed the excellent therapeutic effect of Pri@exo in imiquimod (IMQ)-induced mouse psoriasis model and initially explored its possible therapeutic mechanism. Pri@exo exhibits an excellently targeted ability to alleviate skin psoriatic lesions in mice through anti-inflammatory, anti-ferroptosis, and anti-proliferative mechanisms. To the best of our knowledge, this is the first study on the application of tumor-derived exosomes to inflammatory diseases, as well as the first report on targeting drug delivery through PD-1/PD-L1 interaction to improve the treatment of psoriasis.

Results

Upregulation of PD-1 in psoriasis in vitro and in vivo

To investigate PD-1 expression in psoriatic-like skin lesions, we first used human keratinocytes HaCaT cells induced by tumor necrosis factor-α (TNF-α) as an *in vitro* model of psoriatic dermatitis. The expression of PD-1 was detected using flow cytometry after TNF-α stimulated HaCaT cells for 24 h to induce overactive proliferation. As displayed in Fig. 1A, PD-1 expression on TNF-α-induced HaCaT cells is significantly increased compared with that without TNF-α stimulation.

Next, we used an IMQ-induced mouse psoriasis model to investigate PD-1 expression *in vivo*. Immunohistochemical staining was performed on psoriatic tissue samples using specific anti-PD-1 antibodies. A strong infiltration of immune cells was observed in the skin of IMQ-treated mice but not Vaseline-treated mice. (Fig. 1B). Meanwhile, a significant increase in PD-1 expression was observed in IMQ-treated mice compared with control mice (Fig. 1B). Furthermore, a more detailed expression of PD-1 on lymphocytes was carried out. Compared with the control group, the expression of PD-1 on $CD11b^+$ cells and $CD4^+$ T cells infiltrated in the skin from IMQ-treated mice were increased by 2.5 times and 1.6 times, respectively, as revealed by immunofluorescence staining (Figs. 1C and D). We also investigated the expression of PD-1 in the spleen during IMQ-induced psoriatic inflammation. The spleen from mice treated with or without IMQ was harvested to determine PD-1 expression on $CD11b^+$ cells, $CD4^+$ T cells, and $CD8^+$ T cells using flow cytometry. Consistent with the data obtained with immunofluorescence staining, the PD-1 expression on $CD11b^+$ cells and $CD4^+$ T cells in the spleens from the IMQ-treated mice exhibited higher expression (Figs. 1E and F) compared with the control group. Concomitantly, no significant difference was noted between the control and IMQ-treated groups in PD-1 expression on $CD8^+$ T cells (Fig. S1). Collectively, these data confirmed that PD-1 is overexpressed by HaCaT cells, $CD11b^+$ cells, and $CD4^+$ T cells in models of psoriasis. T helper 17 (Th17) cells are specialized CD4 + effector T cells that primarily produce IL-17, which plays a crucial role in the pathogenesis of psoriasis[12]. Besides, CD11b is a pan-myeloid innate lymphoid cell marker predominantly expressed in various cell types, including neutrophils, monocytes, macrophages, and dendritic cells, which are activated in psoriasis, contributing to disease pathology through IL-17-dependent and IL-17-independent mechanisms[13, 14]. Overall, our data supported the overexpression of PD-1 on keratinocytes and lymphoid cells, including innate and $CD4^+$ cells, indicating that PD-1 had a broad perspective as a potential therapeutic target in treating psoriasis.

Formulation and characterization of Pri@exo

Given that PD-1 is significantly elevated on several cell types that play an important role in the pathogenesis of psoriasis, we attempted to develop a drug delivery system targeting PD-1 to improve the treatment of psoriasis. Considering that the natural ligand of PD-1 is PD-L1, and PD-L1 is overexpressed on the surface of various tumor cells such as melanoma cells and its derived exosomes, we tried to explore the use of tumor-derived exosomes to target drug delivery through PD-1/PD-L1 specific interaction. We utilized exosomes derived from B16F10 murine melanoma cells as a targeted drug delivery platform. Exosomes derived from B16F10 cell lines were isolated and purified from the culture medium by ultracentrifuge, as described in the Methods section.

Pristimerin is a bioactive natural quinone triterpenoid with excellent anti-inflammatory activity, but its clinical application is limited because of its poor water solubility. To improve its water solubility, pristimerin nanodots with a diameter of 15.2 ± 3.4 nm (Fig. 2A) were successfully prepared using a brilliant droplet-confined/cryodesiccation-driven crystallization approach[15]. Pristimerin nanodots were next encapsulated into the exosomes through ultrasonic and incubation[16] (Pri@exo). The known

exosome biomarkers, including tumor susceptibility gene 101 protein (TSG101) and CD63, were both detected in exosome and Pri@exo (Fig. 2B). Furthermore, the high levels of PD-L1 on exosomes and Pri@exo are evidenced in Fig. 2B. Representative transmission electron microscopy (TEM) images revealed that the exosomes or Pri@exo yielded a known characteristic morphology for exosomes, where a central depression was observed (Fig. 2A). The atomic force microscopy (AFM) images of Pri@exo depicted a typical oval structure of exosomes, and the pattern of exosomes in three-dimensional imaging in an oblique view (Fig. 2C). Dynamic light scattering analysis displayed that the size of the exosomes and Pri@exo were 87.49 ± 14.90 nm and 89.56 ± 26.35 nm, respectively, and their particle sizes were not significantly different (Figs. 2D and E). The ultraviolet-visible absorption spectra of pristimerin nanodots and Pri@exo depicted the appearance of a characteristic absorption band centered at 460 nm, indicating that pristimerin was efficiently loaded into exosomes (Fig. 2F). Obviously, the encapsulation of pristimerin nanodots did not affect the feature, morphology, and diameter distribution of exosomes. Pri@exo was loaded into Pluronic F127 thermosensitive injectable hydrogel to improve controlled delivery. The Pluronic F127 hydrogel loaded with Pri@exo could gel rapidly at 37°C (Fig. 2G). These findings indicate that Pri@exo was successfully prepared for further application.

Excellent PD-1-target capability of Pri@exo

To investigate the cellular internalization process of Pri@exo in $CD4^+$ T cells, $CD4^+$ T cells isolated from healthy mice or IMQ-induced mice were incubated with Cy5.5-labeled Pri@exo for 0.5, 1, 2, 4, and 6 h. The results at multiple time points after the co-incubation of Pri@exo and $CD4^+$ T cells derived from different mice revealed that the uptake of Pri@exo by $CD4^+$ T cells by IMQ-induced mice was much higher than that of healthy mice (Fig. 3A). Quantitatively, the mean fluorescence intensity was markedly higher in $CD4^+$ T cells from IMQ-induced mice than in $CD4^+$ T cells from healthy mice at indicated time points (Fig. 3B). Moreover, the results from confocal laser scanning microscope images supported the previous observation regarding higher uptake of Pri@exo $CD4^+$ T cells by IMQ-induced mice (Fig. 3C). Considering that PD-1 is overexpressed in active $CD4^+$ T cells, it is reasonable for Pri@exo to display the high-efficiency endocytosis. Likewise, the cellular uptake of Pri@exo by HaCaT cells was also evaluated using flow cytometry (Figs. 3D and E). The mean fluorescent intensity value of TNF-α-induced HaCaT cells was higher than that of the control group. These findings strongly indicated that Pri@exo displays strong cellular uptake and intracellular retention in active $CD4^+$ T cells and HaCaT cells, suggesting the $PD\text{-}1^+$ cells targeting capacity of Pri@exo.

Next, we investigated the biodistribution of Pri@exo hydrogel *in vivo*. To facilitate tracking, a near-infrared fluorescent dye Cy5.5 was labeled to Pri@exo. The Cy5.5-labeled Pri@exo hydrogel was subcutaneously injected into the back skin of mice, and the fluorescent signal intensity at different time points was monitored by a fluorescent imaging system. Although the fluorescence signal of Cy5.5-labeled Pri@exo hydrogel decreased with time, it remained *in vivo* for up to 48 h (Figs. 3F and S2), achieving a slow, sustained release. The *ex vivo* biodistribution studies demonstrated a low accumulation of Pri@exo in all major organs (heart, liver, spleen, lung, and kidney; Fig. S3). Furthermore, the efficient accumulation of

Pri@exo in the draining lymph nodes 12 h after injection indicated that Pri@exo could actively target subcutaneous lymph nodes (Fig. S4).

Superior in vitro anti-Inflammation of Pri@exo

Previous studies have demonstrated that pristimerin and its analogs can modulate immune homeostasis and inhibit T cell activation in various mouse models of inflammation[17, 18]. Moreover, PD-L1$^+$ exosomes secreted by tumors suppress T cell activity in the tumor immune microenvironment[19]. To verify whether Pri@exo can stabilize CD4-mediated immune balance or not, we investigated the effect of Pri@exo on CD4$^+$ T cell activation and differentiation *in vitro*. The naïve CD4$^+$ T cells isolated and purified from the spleen of BALB/C mice by magnetic-activated cell sorting were stimulated with TGF-β and IL-23, exposed to various treatments for 72 h, and finally analyzed using flow cytometry. Figures 4A, B, and D display significant differences in the percentage of Th17 and Tregs among the CD4$^+$ T cells with various treatments. Compared with the groups treated with Pristimerin or exosomes, Pri@exo with the most prominent ability to downregulate the expression of IL-17 in CD4$^+$ T cells and augment the frequency of Tregs, which indicated that Pri@exo enhanced the therapeutic efficacy of pristimerin or exosomes *in vitro*. TNF-α served as pro-inflammatory cytokines in both the initiation and the amplification of psoriasis[4, 20]. We observed the most pronounced anti-psoriasis effect in Pri@exo group with a significantly decreased expression of TNF-α from 2.96% (mock group) to 1.21% (Pri@exo group; Figs. 4C and D). These results indicated that tumor-derived exosomes and pristimerin nanoparticles significantly inhibited the expression of inflammatory mediators from CD4$^+$ T cells mediated by IL-23 and promoted the differentiation of CD4$^+$ T cells into Tregs, while Pri@exo exhibited a more excellent synergistic effect.

Enhanced anti-psoriasis effects of Pri@exo in psoriasis

Based on the above responses, we chose Pri@exo as a therapeutic agent to investigate anti-psoriatic effects *in vivo* by IMQ-induced psoriasis-like skin inflammation model. Pri@exo hydrogel was subcutaneously injected on shaved back skin every two days, followed by IMQ cream 4 h later. We visually observed that IMQ group exhibited apparent erythema, scaling, and infiltration for seven days, while Pri@exo administration attenuated skin lesion severity (Fig. 5A). The characteristic signs of IMQ-induced skin lesions, including scaling, erythema, and infiltration, were scored daily using a scoring system based on the psoriasis area and severity index known as Baker score. Besides, a significant change in the skin was observed according to the Baker score (Fig. 5B). Next, skin samples were fixed and stained using a standard hematoxylin and eosin (H&E) method to analyze histological changes. Typical histopathological changes of psoriasis are characterized by hyperkeratosis, parakeratosis, modest acanthosis, elongated rete ridges, and modest dermal inflammation[21]. It is revealed in Fig. 5C and D that the mice in IMQ group exhibited extensive psoriasiform lesions, while treatment with Pri@exo significantly alleviated the severity of skin lesions. Furthermore, the thickness of epidermis in the IMQ group was 110–140 μm. However, the value of epidermal thickness significantly decreased in the Pri@exo group with the range from 40 to 70 μm (Fig. 5E).

Most clinical features of psoriasis, such as keratinocyte hyperproliferation, neovascularization, and increased inflammation, could be attributed to cytokines expressed in psoriatic skin. The interleukins (IL), in particular, IL-6, IL-12, and IL-23, have been specifically implicated as key players in the pathogenesis of psoriasis. Therefore, we examined the expressions of these inflammatory cytokines in plasma. The pro-inflammatory cytokines, including IL-6, IL-12, and IL-23, significantly increased in the IMQ group compared with the untreated mice, and Pri@exo treatment had a pronounced effect in downregulating the secretion of inflammatory cytokines (Fig. 5F). In conclusion, the administration of Pri@exo not only alleviated the clinical symptoms but also decreased the inflammation of IMQ-induced psoriasis.

We next characterized the influence of Pri@exo treatment on immune cells from IMQ-induced psoriasis mice using flow cytometry and immunohistochemistry. Compared with IMQ group, the numbers of $CD4^+$ T cells in the spleen and draining lymph nodes significantly decreased upon Pri@exo treatment, mirroring the homeostatic imbalance in the untreated mice (Figs. 6A and B). Data from the immunofluorescence assay in the psoriasis skin demonstrated that the intense infiltration of $CD3^+$ T cells was fiercely decreased by Pri@exo treatment (Fig. S5). While the number of $CD8^+$ T cells appeared less responsive in the IMQ-induced psoriasis model, Pri@exo reduced the number of $CD8^+$ T cells in the draining lymph nodes to a greater extent than in the spleen.

In psoriasis, activated macrophages are also believed to provoke skin lesions and contribute to T cell-mediated pathways of inflammation[22]. The number of macrophages (represented by $F4/80^+$ $CD11b^+$ cells) in both spleen and draining lymph nodes highly increased after IMQ stimulation. We found that Pri@exo attenuated or even counteracted the increase in macrophages induced by IMQ in the spleen or draining lymph nodes (Fig. 6C and D). Furthermore, the change of $CD206^+$ M2-like macrophages in different groups was examined. CD206 expression on macrophages was significantly lower in the IMQ group than in the control group (Figs. 6E and F). However, Pri@exo treatment upregulated the expression of CD206 on macrophages (Figs. 6E and F). High expression of CD206 contributed to the conversion of macrophages into an anti-inflammatory M2 phenotype that suppressed inflammation. The increase in M2-like macrophages induced by Pri@exo in IMQ-induced psoriasis indicates a better prognosis.

To further verify whether Pri@exo can mediate other innate immune cells, immunohistochemistry was used to determine neutrophils (represented by $Ly6G^+$ cells) and dendritic cells (represented by $CD11c^+$ cells). Pri@exo substantially reduced the migration of neutrophils and dendritic cells into affected skin areas compared with mice treated with IMQ (Figs. 6G). These results suggested that *in vivo* anti-psoriasis effects of Pri@exo were associated with negative regulation of various immune cell activities.

Consistently, the expression of PD-1 in skin tissue of Pri@exo-treated mice was significantly reduced, indicating that the pathological process of psoriasis is inhibited. In addition, we also observed Ki67 and PCNA, two key parameters in cell proliferation. We found that both Ki67 and PCNA expressions were significantly increased in the psoriasis group, indicating abnormally proliferating keratinocytes, which were effectively inhibited by pri@exo (Figs. 7A and B). Under physiological conditions, the proliferation of keratinocytes in the skin is a tightly controlled process. In psoriasis, however, the control mechanisms go

away, resulting in keratinocytes' overgrowth, mis-differentiation, and increased migratory capacity[23]. To assess the effect of Pri@exo on the proliferation of HaCaT cells, we performed a carboxifluorescein diacetate succinimidyl ester (CFSE) dilution assay using flow cytometry. A more robust proliferation of HaCaT cells was observed, while Pri@exo-treated HaCaT had 3.3 times and 1.7 times lower proliferation than those in exosomes or pristimerin nanoparticle group (Fig. 7C).

Keratinocyte death contributes to the amplification of the inflammatory cascade during psoriatic inflammation[24, 25]. A recent study reported that ferroptosis, a programmed non-apoptotic form of cell death, is implicated in the pathogenesis of psoriasis[26]. To explore whether Pri@exo affected ferroptosis-related cell death in psoriatic lesions, the expression levels of ferroptosis-related proteins, including 4-hydroxynonenal (4-HNE), glutathione peroxidase 4 (GPX4), and Acyl-CoA synthetase long-chain family member 4 (ACSL4), were detected in psoriatic lesions and normal samples using immunofluorescent staining (Fig. 7D). In the psoriatic skin, the intensity of 4-HNE, the primary byproduct of lipid peroxidation, was conspicuously elevated compared to normal skin, whereas Pri@exo administration markedly reduced the formation of 4-HNE. Meanwhile, in the basal layer of the psoriatic epidermis, an essential pro-ferroptotic enzyme ACSL4 was strongly upregulated, and GPX4 was barely observed. Treatment with Pri@exo attenuated this phenotype to a certain extent compared to the IMQ group. Consistently, western blot displayed a significant reduction in the expression of 4-HNE, ACSL4, and a slight increase of GPX4 in psoriatic samples of Pri@exo group than the IMQ group (Figs. 7E and F). These data suggested that Pri@exo alleviated psoriatic inflammation through suppression of keratinocyte ferroptosis.

Extremely low systematic toxicity of Pri@exo

Owing to the complex composition and undetermined biological functions of tumor-derived exosomes, their safety issues still require additional attention and analysis. To investigate the systematic toxicity of Pri@exo *in vivo*, we subcutaneously injected the same therapeutic dose of Pri@exo hydrogel in BALB/c healthy mice for seven days, after which major organs were harvested for the histopathological examination and blood was collected for biochemical analysis. The H&E staining of sliced heart, liver, spleen, lung, and kidney showed no morphological changes in Pri@exo group compared to the control group (Fig. 8A). Besides, the hematological profile depicted that the levels of Alanine aminotransferase(ALT), aspartate aminotransferase(AST), albumin(ALB,)total bilirubin(TBIL), uric acid(UA), blood urea nitrogen(BUN), creatinine(Cr), and γ-glutamyl transferase(γ-GT) in Pri@exo-treated mice remained within the normal range or comparable to the control mice (Fig. 8B), indicating that treatment with Pri@exo did not induce significant hematological toxicity. During the dosing period, the body weight of Pri@exo-treated mice did not change significantly compared to untreated mice (Fig. S6). All the results contributed to serving Pri@exo as a safe nano-formulation for psoriasis.

Discussion

Despite intensive research, current pharmacologic treatments for psoriasis are far below satisfactory[2]. In the present study, we developed a treat-to-target strategy based on tumor-derived PD-L1^{+} exosomes as

a bio-inspired nanocarrier for anti-inflammatory pristimerin to ameliorate IMQ-induced psoriasiform inflammation in mice. Pri@exo could target activated $CD4^+$ T cells and keratinocytes via PD-1/PD-L1 interaction during the inflammatory progression of psoriasis, thereby inhibiting keratinocyte ferroptosis and attenuating the inflammatory cascade. This ultimately decreased the abnormal proliferation of keratinocytes in psoriatic lesions.

The PD-1/PD-L1 interaction is an important immunosuppressive signaling pathway within the tumor microenvironment[27]. The dramatic efficacy of PD-1/PD-L1 blockade in cancer immunotherapy prompts the control of other autoimmune diseases by PD-1 signal modulation[28]. Previous studies have reported that PD-1 is overexpressed by IL-17A–producing T cells in both IMQ-treated mice[29] and human psoriatic skin. Recombinant PD-L1 alleviated IMQ-induced psoriatic inflammation in mice, and the genetic deficiency of PD-1 aggravated psoriatic inflammation[30, 31]. In the clinic, anti-PD-1/PD-L1 therapies are implicated with a risk of new-onset psoriasis and exacerbating pre-existing psoriatic skin lesions[32]. Consistently, our results show that the expression of PD-1 on $CD4^+$ T cells and keratinocytes was highly regulated during inflammation in IMQ-induced psoriasis, making it a specific target for drug delivery. As expected, PD-$L1^+$ exosomes derived from tumor cells exhibited efficient uptake and retention in active $CD4^+$ T cells and HaCaT cells. In addition to their inherent immunosuppressive effect, PD-$L1^+$ exosomes may serve as an effective active targeting nanoscale carrier to accomplish anti-inflammatory drug delivery. Here we observe a marked additive effect of Pri@exo, with superior efficacy over single PD-$L1^+$ exosome and pristimerin.

Conventional construction of targeted nanoparticles usually requires complex synthesis and surface modification, which is often toxic. Also, the possible introduction of foreign components is highly susceptible to unknown toxic side effects[33, 34]. The exosomes we prepared are natural nanoparticles from B16F10 melanoma cells with good biocompatibility and high tolerance. Our results demonstrated that loading tumor-derived exosome with pristimerin is a feasible, relatively safe, and effective therapeutic option for psoriasis. Additionally, recent studies have reported that melanoma-derived PD-L1-rich exosomes can combine with PD-1 on the surface of T cells with immunosuppressive effects, causing T cell dysfunction or exhaustion[35], which suggest unique advantages as drug carriers or components in inflammatory diseases[36, 37]. Here we analyzed the immunosuppressive activity of Pri@exo and explored the underlying mechanism in our preliminary experiment. Pri@exo is efficiently internalized into target cells, resulting in the strongest inhibition of IL-17 and TNF-α secreted by $CD4^+$ T cells and the highest inhibition of proliferation in keratinocytes than other groups. Furthermore, in psoriasis, Tregs are readily converted into cells that express IL-17, thus potentially perpetuating the inflammatory process of the disease[38, 39]. Pri@exo could substantially reverse the reduction of Treg mediated by the pro-inflammatory factor IL-23 compared to the exosome-treated and pristimerin-treated groups. Notably, Pri@exo is not only slowly released in the skin after subcutaneous injection but also effectively accumulated in the draining lymph nodes, both of which are the main sites of immune microenvironment homeostasis imbalance in psoriasis[40]. Impairment and death of keratinocytes have been implicated in the pathogenic mechanisms of psoriasis, which act as a primary initiator to amplify the inflammatory

cascade by releasing immunogenic intracellular molecules and activating inflammasomes[41, 42]. Recently, several studies found that keratinocyte ferroptosis was intricately linked to skin inflammation. Inhibition of ferroptosis prevented the release of damage-associated molecular patterns from the epidermal keratinocytes[43] and blocked psoriasis inflammation in mice[26]. Consistent with this, we also observed a similar tendency of ferroptosis in IMQ-induced psoriasis mice. Of interest, Pri@exo treatment could notably inhibit ferroptotic cell death of psoriatic keratinocytes. We speculated that Pri@exo diminishes psoriatic inflammatory responses, which is, in part, ascribable to the inhibition of keratinocyte ferroptosis, thereby attenuating the activation of inflammatory signaling cascades. The unique in *vivo* biodistribution properties of Pri@exo facilitate its excellent anti-psoriatic effects.

Conclusions

Current PD-1/PD-L1-mediated targeted therapy strategies utilizing tumor-derived exosomes can precisely deliver anti-inflammatory drugs pristimerin to PD-1$^+$ immune cells and keratinocytes, which has been demonstrated not only to relieve the typical symptoms of psoriasis by deactivating various abnormal innate and adaptive immune cells but also to inhibit ferroptotic cell death of psoriatic keratinocytes, thereby improving therapeutic efficacy. Meanwhile, Pri@exo, with good biocompatibility and biodegradability, shows no obvious toxic effect in healthy BABL/C mice and could be effectively cleared from the body by natural means without causing long-term accumulation or chronic toxicity. Our results support that Pri@exo has an inflammatory tropism and excellent anti-inflammatory effect, which can also be extended to treating various inflammatory diseases.

Materials And Methods

Materials and reagents

Dulbecco's modified Eagle medium (DMEM), RPMI 1640, and fetal bovine serum (FBS) were purchased from Biological Industries (Kibbutz Beit Haemek, Israel). Pristimerin (98.0%) was purchased from Shanghai Yuanye Bio-Technology Co., Ltd (Shanghai, China). Cy5.5-NHS were purchased from MedChemExpress (New Jersey, USA). Pluronic F-127 was purchased from Sigma-Aldrich (St. Louis, USA). Penicillin/streptomycin antibody mixture (100x), DAPI staining buffer, and RIPA lysis buffer were purchased from Beyotime Biotechnology (Shanghai, China). Phosphate buffer solution (PBS) was purchased from Beijing Solarbio Science & Technology Co., Ltd. (Beijing, China). Naïve CD4$^+$ T isolation kit was purchased from Novus Biologicals (California, USA). ExoEasy Maxi Kit was purchased from Qiagen Biotechnology (MD, USA). 3,3'-diaminobenzidine (DAB) assay kit and BCA protein assay kit was purchased from Servicebio (Wuhan, China). Enzyme-linked immunosorbent kits for cytokines (IL-12 and IL-23) were purchased from Meimian (Jiangsu, China). Polyvinylidene fluoride (PVDF) membrane was purchased from Millipore (MA, USA). The antibodies we used were showed in table 1 with their application and dilution rate. All the chemicals used in this study were of analytical grade.

Cell culture

The mouse melanoma cell line B16-F10 was provided by Prof. Guo Fu, Xiamen University, Xiamen, China. B16-F10 cells were cultured in Dulbecco's modified eagle medium containing 10% exosome-free fetal bovine serum (FBS) and 1% penicillin/streptomycin.

The human epidermal keratinocyte, HaCaT cell line, was a kind gift from Prof. Yin Rui, Department of Dermatology, Southwest Hospital, Third Military Medical University (Army Medical University), Chongqing, China. HaCaT cells were kept in RPMI-1640 medium supplemented with 10% FBS and 1% penicillin/streptomycin. After the cells grew well, TNF-α (100 ng/mL) was added to the culture medium to over-proliferate cells while Pri@exo (20 μg/mL) was added to reverse it[44]. The cells were then harvested for further experiments.

Naïve $CD4^+$T cells were isolated from healthy BLAB/C mouse spleens using naïve $CD4^+$T isolation kit. In brief, spleens were harvested and ground with a syringe on an irony mesh place. Next, red blood cells were removed by red blood cell lysis buffer, and the cell pellet was washed in phosphate buffer saline (PBS). After that, the cell suspension was mixed with a cocktail of various biotin antibodies, including anti-B220 biotin, anti-CD8 biotin, anti-CD25 biotin, anti-CD11b biotin, anti-CD11c biotin, anti-NK1.1 biotin, anti-F4/80 biotin, and anti-Gr-1 biotin. The cells were indirectly magnetically labeled with Anti-Biotin MicroBeads, and then we obtained naïve $CD4^+$ T cells by negative selection from the cell suspension. The purified naïve $CD4^+$ T cells were incubated in RPMI-1640 medium supplemented with 10% FBS (exosome-free FBS), 1% penicillin/streptomycin mixture, and IL-2 (50 ng/mL). After 48 h, IL-23 (20 ng/mL) and TNF-α (50 ng/mL) were added to the culture medium to activate the inflammation reaction while adding Pri@exo (20 μg/mL) to reverse it. The cells were then harvested for further experiments.

All types of cells were incubated in a constant-temperature cell incubator at 37°C, 5% CO ，and 95% air.

Isolation of exosomes

B16-F10 cells were cultured in media supplemented with 10% exosome-free FBS to purify exosomes from the supernatant. Bovine exosomes were depleted by ultracentrifugation at 100,000 g overnight using Optima XPN-100 ultracentrifuge (Beckman Coulter, CA, USA). After 72 h culture, supernatants were harvested, and exosomes were purified by differential centrifugation according to a standard protocol described perviously[35]. Briefly, culture supernatants were centrifuged at 2000 g for 20 min and 16,500 g for 45 min to remove dead cells, cell debris, and micro-vesicles. The supernatants were rotated at 100,000 g for 2 h, and then pellets were suspended in PBS. Exosomes were collected by ultracentrifugation at 100,000 g for 90 min, and the pelleted exosomes were resuspended in 200 μL sterile PBS. All centrifuge processes were performed at 4°C.

Preparation of Pri@exo

Ultra-small pristimerin nanodots were fabricated by droplet-confined crystallization during the freeze-drying of frozen emulsion[15]. Pristimerin-containing dichloromethane was mixed with an aqueous solution containing F127 (1.0 wt.%) and then converted into an O/W emulsion by sonification. The emulsion was immediately immersed in liquid nitrogen and rapidly frozen, followed by freeze-drying. The

resulted in pristimerin nanodots were harvested and washed by centrifugation–redispersion cycles to remove free F127.

Pristimerin nanodots (50 μg) were added to the exosomes (100 μg), and the mixture was sonicated (500 V, 2 kHz, 20% power, five cycles by 5 s pulse and 5 s pause). Next, the mixture was incubated at 4°C overnight. All the procedures were performed on ice. The unloaded drugs were removed by exoEasy Maxi Spin Columns from the exoEasy Maxi Kit.

Characterization of pristimerin nanodots

The morphology of Pristimerin nanodots were observed by transmission electron microscopy (TEM, JEM-1400, JEOL) at 80 kV.

Characterization of Pri@exo

For observation of Pri@exo, the sample was prepared as the previous study described[45]. In brief, 10-μL purified Pri@exo was suspended in PBS and placed on formvar-carbon-coated copper grids. After allowing Pri@exo to be attached to grids for 10 min, the liquid was removed from the edge of grids by filter paper. Pri@exo on the grids was then stained with 2% uranyl acetate for 15 min. Grids were washed with distilled deionized water for 5 s and then air-dried. Pri@exo was imaged by TEM (HC-1, Hitachi) at 80 kV. The size, shape, and morphology of purified Pri@exo were also investigated using atomic force microscopy (Nanoview6600, Veeco-V, Jiangsu, China) employing tapping mode[46]. Briefly, purified Pri@exo was diluted (1:1000) in filtered PBS and spin-coated onto the surface of a freshly cleaved silicon substrate. For the preparation of each measurand, 20 μL of the diluted exosome sample was mounted onto a silicon substrate and spin-coated at 1500 g for 30 s. The images were analyzed using the NanoScope 7.20 (Build R1.30937) software. The mean hydrodynamic diameter of Pri@exo was measured using a Zetasizer Nano ZS (Malvern, UK).

The dual-targetability of Pri@exo

Naïve $CD4^+$ T cells were seeded and incubated in 24-well plates for 24 h and then treated with Cy5.5-loaded Pri@exo under the equivalent concentration (20 μg/mL) for 6 h. Cells were fixed with 4% paraformaldehyde for 15 min at room temperature. Sections were prepared by smear assay according to the method reported previously. Briefly, the cell suspension was smeared in glasses by swabs. After drying the sections, DAPI (5 μg/mL) solution was dropped into glasses to stain nuclei for 5 min at room temperature. Sections were assessed with confocal laser microscopy.

The cellular uptake assay of Cy5.5-labeled Pri@exo in $CD4^+$ T cells and HaCaT cells was quantified by flow cytometry. Naïve $CD4^+$ T cells were seeded and incubated in 24-well plates for 24 h. Then, cells were incubated with Cy5.5-labeled Pri@exo under the equivalent concentration (20 μg/mL). At predetermined times (0.5, 1, 2, 4, and 6 h), cells were suspended in cold PBS and immediately analyzed by a flow cytometer (Fortessa, BD Biosciences). As for the treatment of HaCaT cells, TNF-α-induced HaCaT cells were pretreated with TNF-α (100 ng/mL) for 24 h, and then the Cy5.5-labeled Pri@exo was added into the

complete culture medium of a different group (exosome-free FBS) at predetermined time points. Finally, cells were washed with PBS and analyzed via flow cytometry.

Preparation of psoriasis model and administration of Pri@exo

BLAB/C mice aged 6–8 weeks with an average weight of 20–25 g were purchased from the Experimental Animals Center of the Army Medical University (Chongqing, China). After one week of adaption to the new environment. An area of 2 × 3 cm was shaved from the backs of the mice using hair removal creams to remove the remaining hair. The mice were randomly assigned to three treatment groups, i.e., the control, IMQ, and therapy groups. To establish the IMQ-induced psoriasis-like model, mice were treated with a daily topical dose of 62.5 mg of IMQ-cream (5%; Mingxinlidi, Sichuan, China) on the back for seven consecutive days based on a previous study[47]. The negative control was treated with the same dose of Vaseline cream alone. To investigate the therapeutic effect of Pri@exo against IMQ-induced psoriasis, the therapy group was subcutaneously injected with Pri@exo every two days (50 μg/kg for a week). All mice were housed under standard conditions with a 12 h light/12 h dark cycle and were fed with standard mouse chow and water. The psoriasis area and severity index (PASI), which comprised parameters for skin erythema, scaling, and thickness, was scored daily to assess the condition of the psoriasis-like lesion. The damaged skin, spleen, and lymph nodes were removed from the sacrificed mice on day 7 for further analysis. All procedures were performed following the National Research Council's *Guide for the Care and Use of Laboratory Animals* (8th edition, reviewed 2011) and were approved by the Ethical Committee for Animal Experimentation of the Army Medical University.

Histology

Skin tissues harvested from animals on day 7 were fixed in 4% paraformaldehyde, and cut into 4 μm sections, which were stained with hematoxylin and eosin (H&E). To obtain the Baker score, at least 10 randomly selected ten fields were independently examined under the microscope (Nikon, Tokyo, Japan) at a magnification of ×200. The stander of Baker score was same as previous described[48].

Immunohistochemistry

The skin sections were blocked with 5% BSA for 1 h and incubated with primary antibody at 4 ℃ overnight. After washing three times with PBS, the slides were then stained with a goat anti-rabbit IgG secondary antibody. The results were analyzed using a DAB assay kit. The slides were visualized by a microscope (Olympus BX51, Japan) and the integrated optical density (IOD) was measured using Image-pro plus 6.0 software, and the mean density was calculated by IOD/area.

Immunofluorescence

Tissue sections were blocked and incubated with primary antibody at 4 ℃ overnight. After rinsing with PBS, the samples were stained with the secondary AlexaFluor®488- or AlexaFluor®555-conjugated IgG for 60 min at 37 ℃. Nuclei were stained with DAPI (5 μg/mL). The samples were mounted with glycerol.

The sections were photographed by using a microscope (Olympus BX51, Japan) and representative images were presented.

Western blot

Skin tissues lysed in RIPA lysis buffer for 20 min on ice and total protein content was quantified with a BCA protein assay kit. The denatured samples were resolved by 12% SDS-polyacrylamide gels and electroblotted onto PVDF membranes (Millipore, Billerica, MA, USA) using equipment from Bio-Rad (Hercules, CA, USA). After blocking with 5% skim milk, the membranes were incubated with primary antibodies overnight (12 h) at 4 ℃. Then, membranes were incubated with corresponding secondary horseradish peroxidase-conjugated antibodies for 1 h at 37 ℃ temperature. Finally, the immunoblots were imaged by the chemiluminescence western blot detection system (Bio-Rad ChemiDoc MP, California, USA) and analyzed using ImageLab packages.

Flow cytometric analysis

For cellular membrane staining, the suspended cells were stained with the antibodies CD3, CD4, CD8, CD11c, CD11b, CD25, F4/80, CD206, and PD-1. After washed twice using FACS buffer, a flow cytometer (Beckman Coulter, US) was used to analyze the cells.

For intracellular cytokine staining, cells were activated with a cell stimulation cocktail 1×10^6 cells/well in a 96-well plate and incubated according to the manufacturer's specification. After 5 h, the cells were harvested, incubated with antibodies against mouse CD3, CD4 for surface staining. Then, the cells were fixed with fixation buffer and subsequently stained intracellularly with antibodies against murine TNF-α and IL-17A in Intracellular Staining Permeabilization Wash Buffer. The cells were washed three times and analyzed with FACSCalibur flow cytometer.

For intranuclear cytokine staining, cells were incubated with antibodies against mouse CD3, CD4, and CD25 for surface staining. Next, the cells were fixed with fixation buffer and subsequently stained intranuclearly with antibodies against murine FOXP3 in Intranuclear Staining Permeabilization Wash Buffer. The cells were washed three times and analyzed with FACSCalibur flow cytometer (Beckman Coulter, US). FlowJo software was used for all data analysis.

ELISA

The ELISA kits were used to measure interleukin-6, IL-12 and IL-23 in mice serum according to the manufacture instructions.

Statistical analysis

Quantitative results were expressed as mean ± SD. Statistical differences among groups were checked by One-way ANOVA followed by Newman-Keuls multiple comparisons test or Student's unpaired two-tailed t test from GraphPad Prism 9.0 (GraphPad Software, San Diego, CA, USA). $p < 0.05$ was considered statistically significant.

Abbreviations

TNF-α: tumor necrosis factor-α; Th17: T helper 17; TSG101: tumor susceptibility gene 101 protein; TEM: transmission electron microscopy; AFM:atomic force microscopy; TGF-β:Transforming growth factor-β; IL: interleukins; PASI:Psoriasis area and severity index; CFSE: carboxifluorescein diacetate succinimidyl ester; 4-HNE:4-hydroxynonenal; GPX4: glutathione peroxidase 4; ACSL4Acyl-CoA synthetase long-chain family member 4; ALT:aminotransferase; AST:aspartate aminotransferase; ALB:albumin;TBIL:total bilirubin; UA:uric acid; BUN:blood urea nitrogen; Cr:creatinine; γ-GT: γ-glutamyl transferase; DMEM: Dulbecco's modified Eagle medium; FBS:fetal bovine serum; PBS: Phosphate buffer solution; DAB: 3,3'-diaminobenzidine; PVDF:Polyvinylidene fluoride; H&E:hematoxylin and eosin; IOD: integrated optical density;

Declarations

Acknowledgements

Authors are grateful to their respective institutions for support.

Authors' contributions

HJ performed experiments, analyzed data, wrote the manuscript. TL performed a part of experiments, wrote the manuscript. HZ conceived and performed flow cytometric data analysis. QY and SF performed a part of experiments. JH and ZZ onformed the results and assisted with data analysis. HZ and XC provided valuable discussions. RS edited the manuscript, conceived and designed this study. WS wrote and edited the manuscript, provided funding, conceived and designed this study. All authors read and approved the fnal manuscript.

Funding

This work was supported by the National Natural Science Foundation of China (grant numbers 31900995 and 81571569), Chongqing Talents Program (grant number cstc2022ycjh-bgzxm0111) and the Special Basic Science and Cutting-edge Research Project of Chongqing (grant number cstc2021jcyj-msxmX0788).

Availability of data and materials

All data related to the manuscript are available in the manuscript in the form of fgures.

Declarations

Ethics approval and consent to participate

The study was approved by the Ethics Committee of Third Military Medical University.

Consent for publication

All authors gave their consent for publication.

Competing interests

The authors declare no confict of interest.

References

1. Griffiths CEM, Armstrong AW, Gudjonsson JE, Barker J: **Psoriasis.** *Lancet* 2021, **397:**1301-1315.
2. Rendon A, Schäkel K: **Psoriasis Pathogenesis and Treatment.** *Int J Mol Sci* 2019, **20:**1475.
3. Jyothi SL, Krishna KL, Shirin VKA, Sankar R, Pramod K, Gangadharappa HV: **Drug delivery systems for the treatment of psoriasis: Current status and prospects.** *J Drug Deli Sci Tech* 2021, **62:**102364.
4. Armstrong AW, Read C: **Pathophysiology, Clinical Presentation, and Treatment of Psoriasis A Review.** *JAMA-J Am Med Assoc* 2020, **323:**1945-1960.
5. Menter A, Strober BE, Kaplan DH, Kivelevitch D, Prater EF, Stoff B, Armstrong AW, Connor C, Cordoro KM, Davis DMR, et al: **Joint AAD-NPF guidelines of care for the management and treatment of psoriasis with biologics.** *J Am Acad Dermatol* 2019, **80:**1029-1072.
6. Bakshi H, Nagpal M, Singh M, Dhingra GA, Aggarwal G: **Treatment of Psoriasis: A Comprehensive Review of Entire Therapies.** *Curr Drug Saf* 2020, **15:**82-104.
7. Yang B, Chen Y, Shi J: **Exosome Biochemistry and Advanced Nanotechnology for Next-Generation Theranostic Platforms.** *Adv Mater* 2019, **31:**1802896.
8. Wang J, Chen D, Ho EA: **Challenges in the development and establishment of exosome-based drug delivery systems.** *J Controlled Release* 2021, **329:**894-906.
9. Poggio M, Hu T, Pai C-C, Chu B, Belair CD, Chang A, Montabana E, Lang UE, Fu Q, Fong L, Blelloch R: **Suppression of Exosomal PD-L1 Induces Systemic Anti-tumor Immunity and Memory.** *Cell* 2019, **177:**414-427.
10. Xie F, Xu M, Lu J, Mao L, Wang S: **The role of exosomal PD-L1 in tumor progression and immunotherapy.** *Mol Cancer* 2019, **18:**1-10.
11. Zhao Q, Bi Y, Guo J, Liu YX, Zhong J, Pan LR, Tan Y, Yu XJ: **Pristimerin protects against inflammation and metabolic disorder in mice through inhibition of NLRP3 inflammasome activation.** *Acta Pharmacol Sin* 2021, **42:**975-986.
12. Blauvelt A, Chiricozzi A: **The Immunologic Role of IL-17 in Psoriasis and Psoriatic Arthritis Pathogenesis.** *Clin Rev Allergy Immunol* 2018, **55:**379-390.
13. Dmochowska N, Tieu W, Keller MD, Wardill HR, Mavrangelos C, Campaniello MA, Takhar P, Hughes PA: **Immuno-PET of Innate Immune Markers CD11b and IL-1β Detects Inflammation in Murine Colitis.** *J Nucl Med* 2019, **60:**858-863.

14. Panni RZ, Herndon JM, Zuo C, Hegde S, Hogg GD, Knolhoff BL, Breden MA, Li X, Krisnawan VE, Khan SQ, et al: **Agonism of CD11b reprograms innate immunity to sensitize pancreatic cancer to immunotherapies.** *Sci Transl Med* 2019, **11:**eaau9240.
15. Ni D, Ding H, Liu S, Yue H, Bao Y, Wang Z, Su Z, Wei W, Ma G: **Superior intratumoral penetration of paclitaxel nanodots strengthens tumor restriction and metastasis prevention.** *Small* 2015, **11:**2518-2526.
16. Yang X, Shi G, Guo J, Wang C, He Y: **Exosome-encapsulated antibiotic against intracellular infections of methicillin-resistant.** *Int J Nanomed* 2018, **13:**8095-8104.
17. Lu Z, Jin Y, Chen C, Li J, Cao Q, Pan J: **Pristimerin induces apoptosis in imatinib-resistant chronic myelogenous leukemia cells harboring T315I mutation by blocking NF-kappaB signaling and depleting Bcr-Abl.** *Mol Cancer* 2010, **9:**112.
18. Wu R, Zeng J, Yuan J, Deng X, Huang Y, Chen L, Zhang P, Feng H, Liu Z, Wang Z, et al: **MicroRNA-210 overexpression promotes psoriasis-like inflammation by inducing Th1 and Th17 cell differentiation.** *J Clin Invest* 2018, **128:**2551-2568.
19. Morrissey SM, Yan J: **Exosomal PD-L1: Roles in Tumor Progression and Immunotherapy.** *Trends Cancer* 2020, **6:**550-558.
20. Greb JE, Goldminz AM, Elder JT, Lebwohl MG, Gladman DD, Wu JJ, Mehta NN, Finlay AY, Gottlieb AB: **Psoriasis.** *Nat Rev Dis Primers* 2016, **2:**16082.
21. Tokuyama M, Mabuchi T: **New Treatment Addressing the Pathogenesis of Psoriasis.** *Int J Mol Sci* 2020, **21:**7488.
22. Hou Y, Zhu L, Tian H, Sun H-X, Wang R, Zhang L, Zhao Y: **IL-23-induced macrophage polarization and its pathological roles in mice with imiquimod-induced psoriasis.** *Protein Cell* 2018, **9:**1027-1038.
23. Petit RG, Cano A, Ortiz A, Espina M, Prat J, Muñoz M, Severino P, Souto EB, García ML, Pujol M, Sánchez-López E: **Psoriasis: From Pathogenesis to Pharmacological and Nano-Technological-Based Therapeutics.** *Int J Mol Sci* 2021, **22:**4983.
24. Benhadou F, Mintoff D, Del Marmol V: **Psoriasis: Keratinocytes or Immune Cells - Which Is the Trigger?** *Dermatology* 2019, **235:**91-100.
25. Ippagunta SK, Gangwar R, Finkelstein D, Vogel P, Pelletier S, Gingras S, Redecke V, Häcker H: **Keratinocytes contribute intrinsically to psoriasis upon loss of Tnip1 function.** *Proc Natl Acad Sci USA* 2016, **113:**E6162-E6171.
26. Shou Y, Yang L, Yang Y, Xu J: **Inhibition of keratinocyte ferroptosis suppresses psoriatic inflammation.** *Cell Death Dis* 2021, **12:**1009.
27. Li B, Yan C, Zhu J, Chen X, Fu Q, Zhang H, Tong Z, Liu L, Zheng Y, Zhao P, et al: **Anti-PD-1/PD-L1 Blockade Immunotherapy Employed in Treating Hepatitis B Virus Infection-Related Advanced Hepatocellular Carcinoma: A Literature Review.** *Front Immunol* 2020, **11:**1037.
28. Chamoto K, Al-Habsi M, Honjo T: **Role of PD-1 in Immunity and Diseases.** *Curr Top Microbiol Immunol* 2017, **410:**75-97.

29. Kim JH, Choi YJ, Lee BH, Song MY, Ban CY, Kim J, Park J, Kim SE, Kim TG, Park SH, et al: **Programmed cell death ligand 1 alleviates psoriatic inflammation by suppressing IL-17A production from programmed cell death 1-high T cells.** *J Allergy Clin Immunol* 2016, **137:**1466-1476.
30. Imai Y, Ayithan N, Wu X, Yuan Y, Wang L, Hwang ST: **Cutting Edge: PD-1 Regulates Imiquimod-Induced Psoriasiform Dermatitis through Inhibition of IL-17A Expression by Innate γδ-Low T Cells.** *J Immunol* 2015, **195:**421-425.
31. Kim JH, Choi YJ, Lee BH, Song MY, Ban CY, Kim J, Park J, Kim SE, Kim TG, Park SH, et al: **Programmed cell death ligand 1 alleviates psoriatic inflammation by suppressing IL-17A production from programmed cell death 1-high T cells.** *J Allergy Clin Immunol* 2016, **137:**1466-1476.e1463.
32. Sibaud V, Meyer N, Lamant L, Vigarios E, Mazieres J, Delord JP: **Dermatologic complications of anti-PD-1/PD-L1 immune checkpoint antibodies.** *Curr Opin Oncol* 2016, **28:**254-263.
33. Najahi-Missaoui W, Arnold RD, Cummings BS: **Safe Nanoparticles: Are We There Yet?** *Int J Mol Sci* 2020, **22:**385.
34. Yetisgin AA, Cetinel S, Zuvin M, Kosar A, Kutlu O: **Therapeutic Nanoparticles and Their Targeted Delivery Applications.** *Molecules* 2020, **25:**2193.
35. Chen G, Huang AC, Zhang W, Zhang G, Wu M, Xu W, Yu Z, Yang J, Wang B, Sun H, et al: **Exosomal PD-L1 contributes to immunosuppression and is associated with anti-PD-1 response.** *Nature* 2018, **560:**382-+.
36. Yong T, Zhang X, Bie N, Zhang H, Zhang X, Li F, Hakeem A, Hu J, Gan L, Santos HA, Yang X: **Tumor exosome-based nanoparticles are efficient drug carriers for chemotherapy.** *Nature Communications* 2019, **10:**1-16.
37. Das CK, Jena BC, Banerjee I, Das S, Parekh A, Bhutia SK, Mandal M: **Exosome as a Novel Shuttle for Delivery of Therapeutics across Biological Barriers.** *Molecular Pharmaceutics* 2019, **16:**24-40.
38. Schwarz A, Philippsen R, Schwarz T: **Induction of Regulatory T Cells and Correction of Cytokine Disbalance by Short-Chain Fatty Acids: Implications for Psoriasis Therapy.** *Journal of Investigative Dermatology* 2021, **141:**95-104.e102.
39. Martin DA, Towne JE, Kricorian G, Klekotka P, Gudjonsson JE, Krueger JG, Russell CB: **The Emerging Role of IL-17 in the Pathogenesis of Psoriasis: Preclinical and Clinical Findings.** *Journal of Investigative Dermatology* 2013, **133:**17-26.
40. Kupper TS, Fuhlbrigge RC: **Immune surveillance in the skin: mechanisms and clinical consequences.** *Nat Rev Immunol* 2004, **4:**211-222.
41. Duan X, Liu X, Liu N, Huang Y, Jin Z, Zhang S, Ming Z, Chen H: **Inhibition of keratinocyte necroptosis mediated by RIPK1/RIPK3/MLKL provides a protective effect against psoriatic inflammation.** *Cell Death Dis* 2020, **11:**134.
42. Zhang WJ, Song ZB, Bao YL, Li WL, Yang XG, Wang Q, Yu CL, Sun LG, Huang YX, Li YX: **Periplogenin induces necroptotic cell death through oxidative stress in HaCaT cells and ameliorates skin lesions in the TPA- and IMQ-induced psoriasis-like mouse models.** *Biochem Pharmacol* 2016, **105:**66-79.

43. Vats K, Kruglov O, Mizes A, Samovich SN, Amoscato AA, Tyurin VA, Tyurina YY, Kagan VE, Bunimovich YL: **Keratinocyte death by ferroptosis initiates skin inflammation after UVB exposure.** *Redox Biol* 2021, **47:**102143.
44. Lee Y, Choi HK, N'Deh K PU, Choi YJ, Fan M, Kim EK, Chung KH, An AJH: **Inhibitory Effect of Centella asiatica Extract on DNCB-Induced Atopic Dermatitis in HaCaT Cells and BALB/c Mice.** *Nutrients* 2020, **12:**411.
45. Cizmar P, Yuana Y: **Detection and Characterization of Extracellular Vesicles by Transmission and Cryo-Transmission Electron Microscopy.** *Methods Mol Biol* 2017, **1660:**221-232.
46. Parisse P, Rago I, Ulloa Severino L, Perissinotto F, Ambrosetti E, Paoletti P, Ricci M, Beltrami AP, Cesselli D, Casalis L: **Atomic force microscopy analysis of extracellular vesicles.** *Eur Biophys J* 2017, **46:**813-820.
47. Badanthadka M, D'Souza L, Salwa F: **Strain specific response of mice to IMQ-induced psoriasis.** *J Basic Clin Physiol Pharmacol* 2021, **32:**959-968.
48. Shokrian Zeini M, Haddadi NS, Shayan M, Shokrian Zeini M, Kazemi K, Solaimanian S, Abdollahifar MA, Hedayatyanfard K, Dehpour AR: **Losartan ointment attenuates imiquimod-induced psoriasis-like inflammation.** *Int Immunopharmacol* 2021, **100:**108160.

Figures

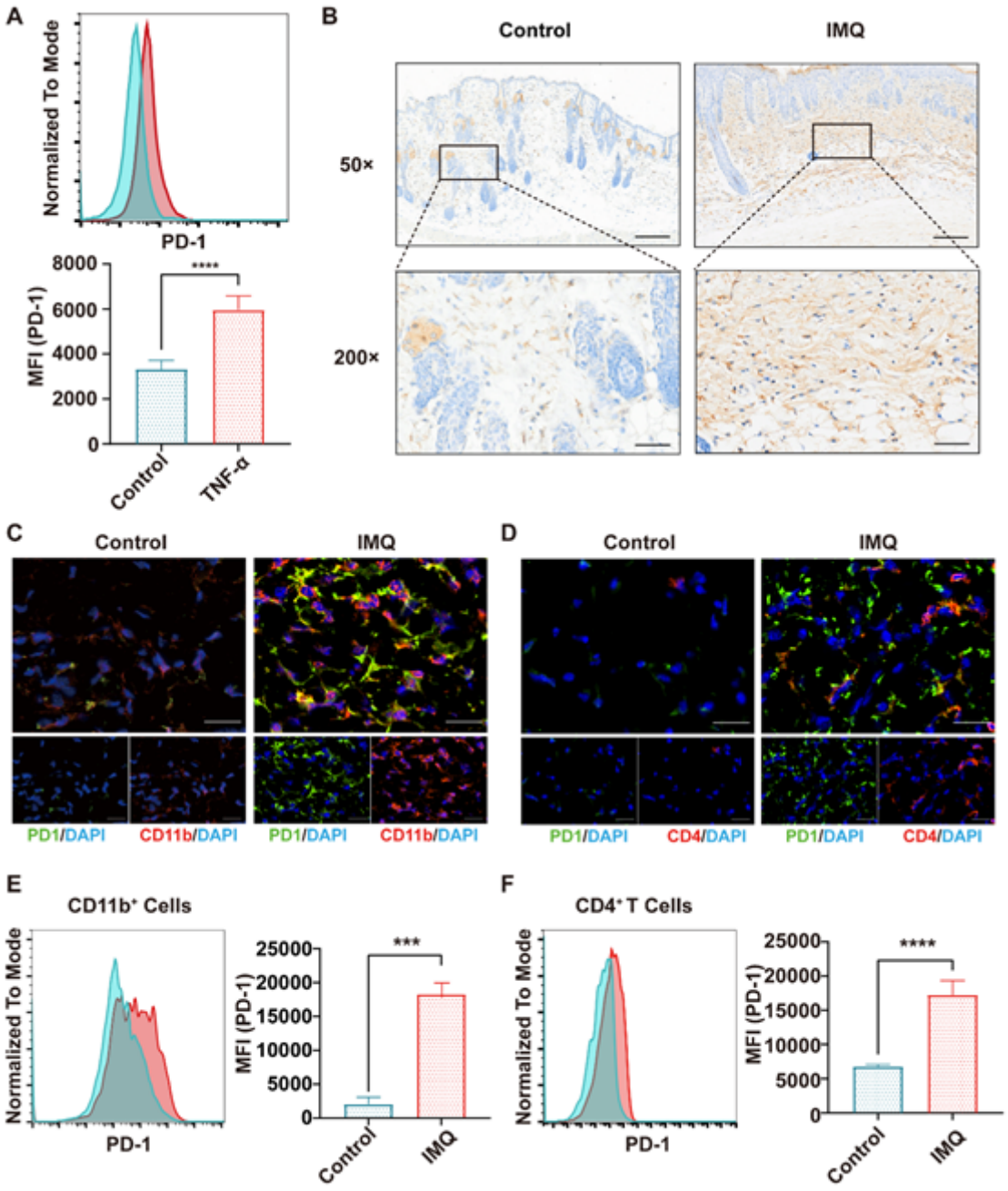

Figure 1

Upregulation of programmed cell death protein 1 (PD-1) expression in imiquimod (IMQ)-induced psoriasis and TNF-α-induced HaCaT cells. (A) Representative flow cytometry histograms (top row) and quantitative analysis (bottom row) of PD-1 expression in HaCaT cells. (B) Skin from a mouse treated with or without IMQ was assayed for PD-1 expression by immunohistochemical staining (magnification, ×50 and ×200; scale bars, 200 and 50 μm, respectively). (C–D) Skin from a mouse treated with or without IMQ used for immunofluorescence (IF) staining with antibodies against CD11b or CD4 (red) plus PD1 (green) and cell nuclei was counterstained with DAPI (blue). (E and F) Representative flow cytometry histograms and quantitative analysis of PD-1 expression in $CD11b^+$ cells (E) and $CD4^+$ T cells (F). The data are expressed as mean ± SD (n = 4 per group). ***p < 0.01, ****p < 0.001.

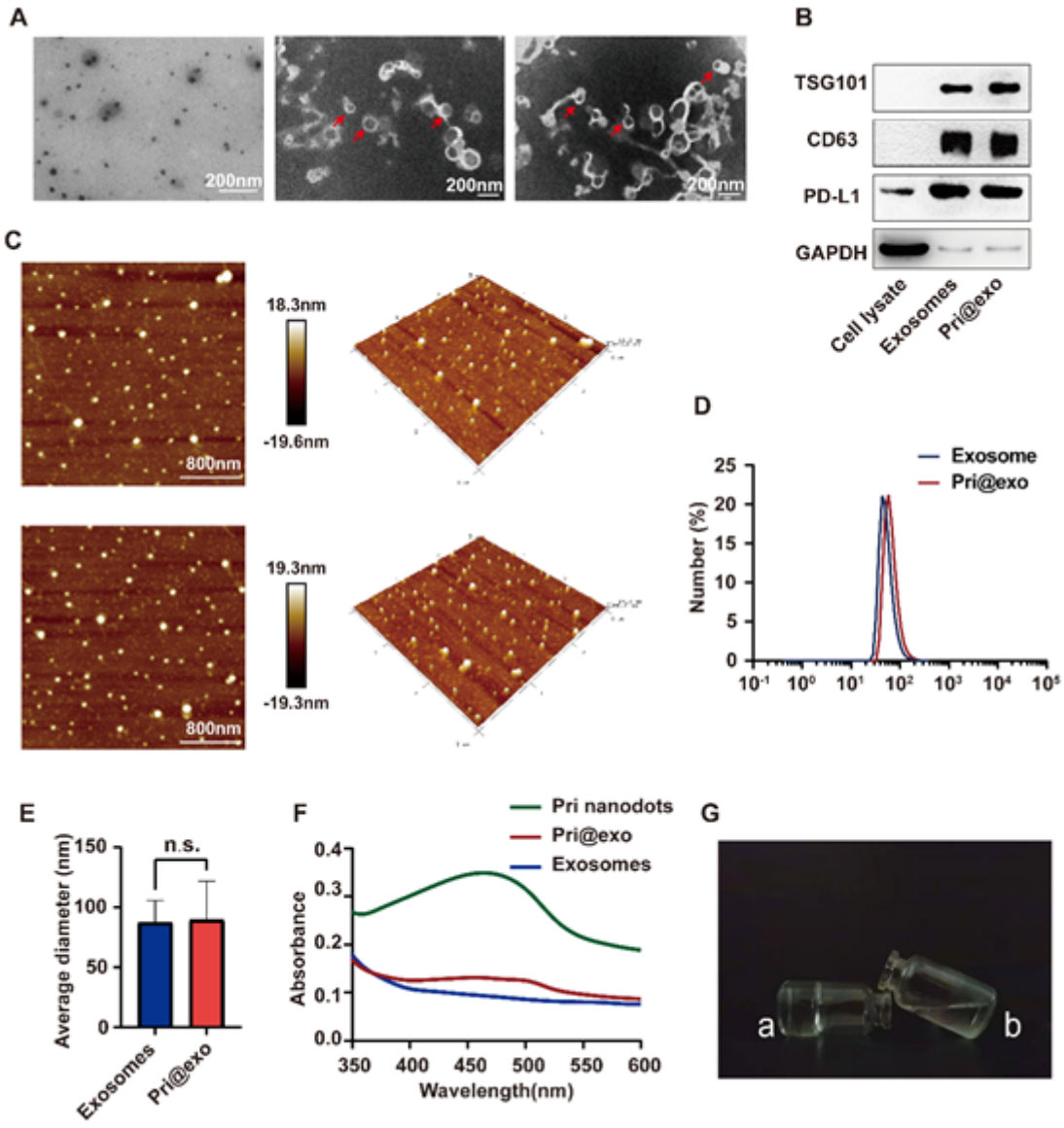

Figure 2

Characterization of Pri@exo. (A) Transmission electron microscopy (TEM) images of pristimerin nanodots (left), exosomes (middle), and Pri@exo (right). Red arrows indicate representative exosomes and Pri@exo. (B) Western blot analysis for PD-L1, CD63, TSG101, and GAPDH in the cell lysates, exosomes, and Pri@exo. (C) Atomic force microscope (AFM) images of exosomes (top row) and Pri@exo (bottom row). (D) Hydrodynamic diameters of exosomes and Pri@exo. (E) The quantitative analysis of the average diameter of exosomes and Pri@exo. (F) Encapsulation of pristimerin onto exosomes as monitored with UV-vis spectra for free nano-pristimerin, exosomes, and Pri@exo. (G) The state of 30% pluronic F127 (PF127) changes temperature-dependently. PF-127 hydrogel (left) at room temperature and PF-127 solution (right) at 4 °C. The data are expressed as mean ± SD (n = 3 per group). n.s., no significance.

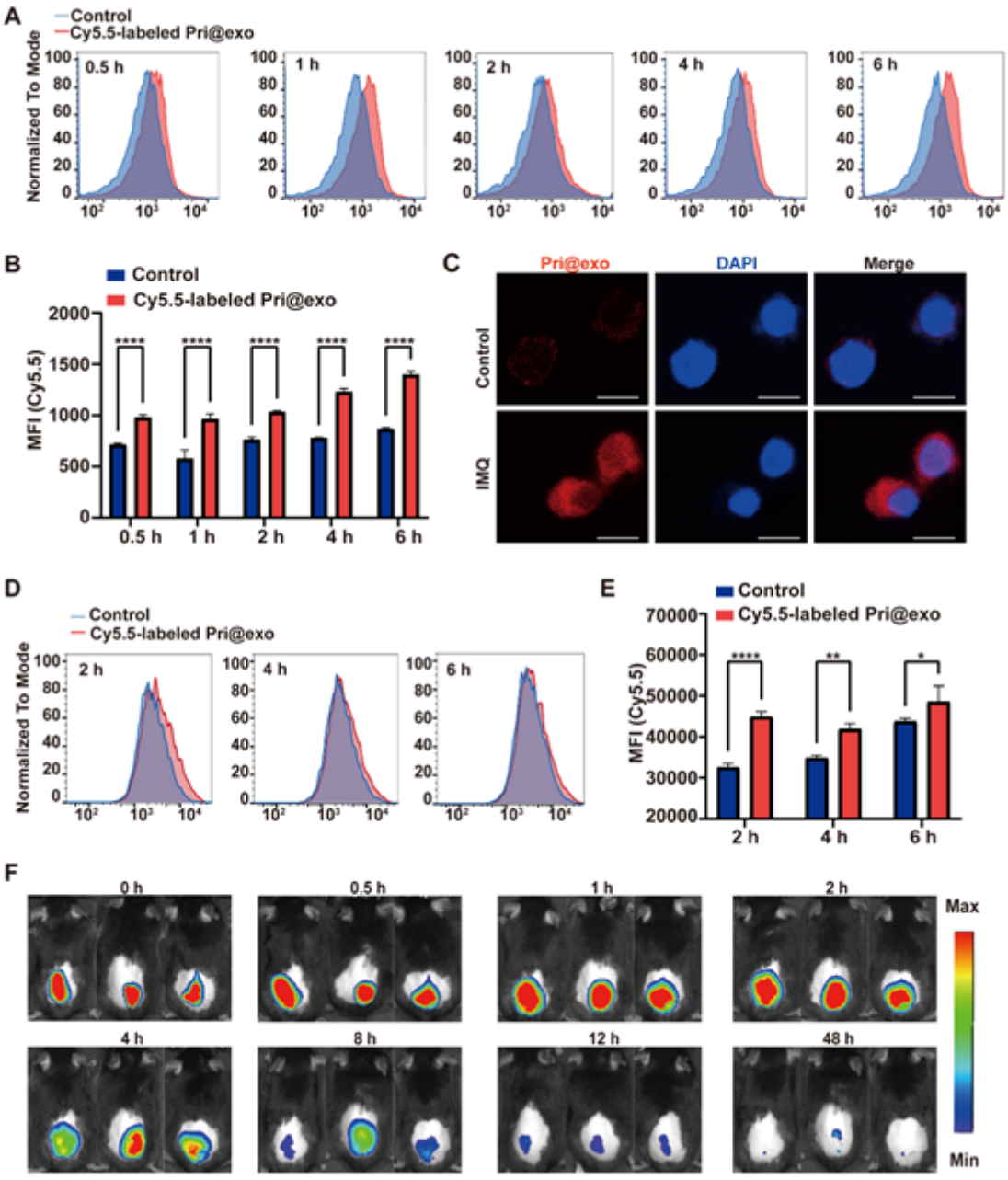

Figure 3

Dual-targeting ability of Pri@exo in keratinocytes and CD4$^+$ T cells *in vitro*. (A) Flow cytometric analysis of CD4$^+$ T cells with or without TNF-α&IL-23 treated with Cy5.5-labeled Pri@exo for 0.5, 1, 2, 4, and 6 h at 37 °C. (B) The quantitative analysis of mean fluorescence intensity in CD4$^+$ T cells. (C) Confocal laser scanning microscope images of CD4$^+$ T cells from the control or IMQ group incubated with Pri@exo for 6 h. Pri@exo was loaded and labeled with Cy5.5 (red), and cell nuclei were counterstained with DAPI (blue). Scale bar, 5 μm. (D) *In vitro* cellular uptake of Cy5.5-labeled Pri@exo in HaCaT cells stimulated with or without TNF-α measured by flow cytometry at selected time points. (E) The quantitative analysis of mean fluorescence intensity in CD4$^+$ T cells. (F) Time course of live-animal fluorescence imaging at indicated

time points post subcutaneous Cy5.5-labeled Pri@exo. The data are expressed as mean ± SD (n = 3 per group). *p < 0.05, **p < 0.01, ****p < 0.001.

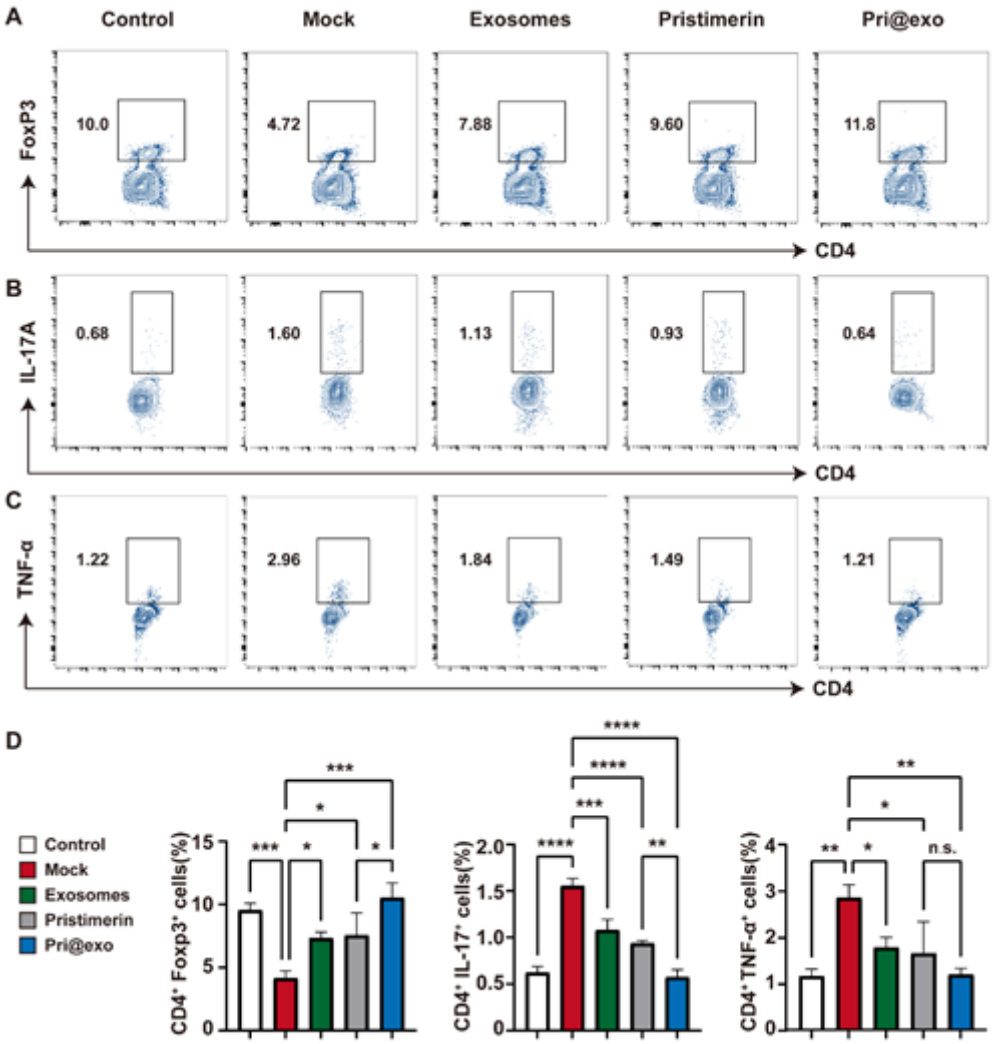

Figure 4

Anti-psoriasis efficacy of Pri@exo *in vitro*. The purified $CD4^+$T cells from male BALB/C mice were cultured with TGF-β (20 ng/mL), TNF-α (50 ng/mL), and IL-23 (20 ng/mL) for 72 h in the presence of pristimerin nanodots, exosomes, and Pri@exo. (A) The representative flow cytometry of FoxP3 expression in $CD4^+$ T cells (Treg). (B and C) The representative flow cytometry of IL-17 (Th17) and TNF-α expression in $CD4^+$ T cells. (D) The percentages of Treg, Th17, and TNF-α expression in CD4+T cells. The data are expressed as mean ± SD (n = 3 per group). *p < 0.05, **p < 0.01, ***p < 0.01, ****p < 0.001, n.s., no significance.

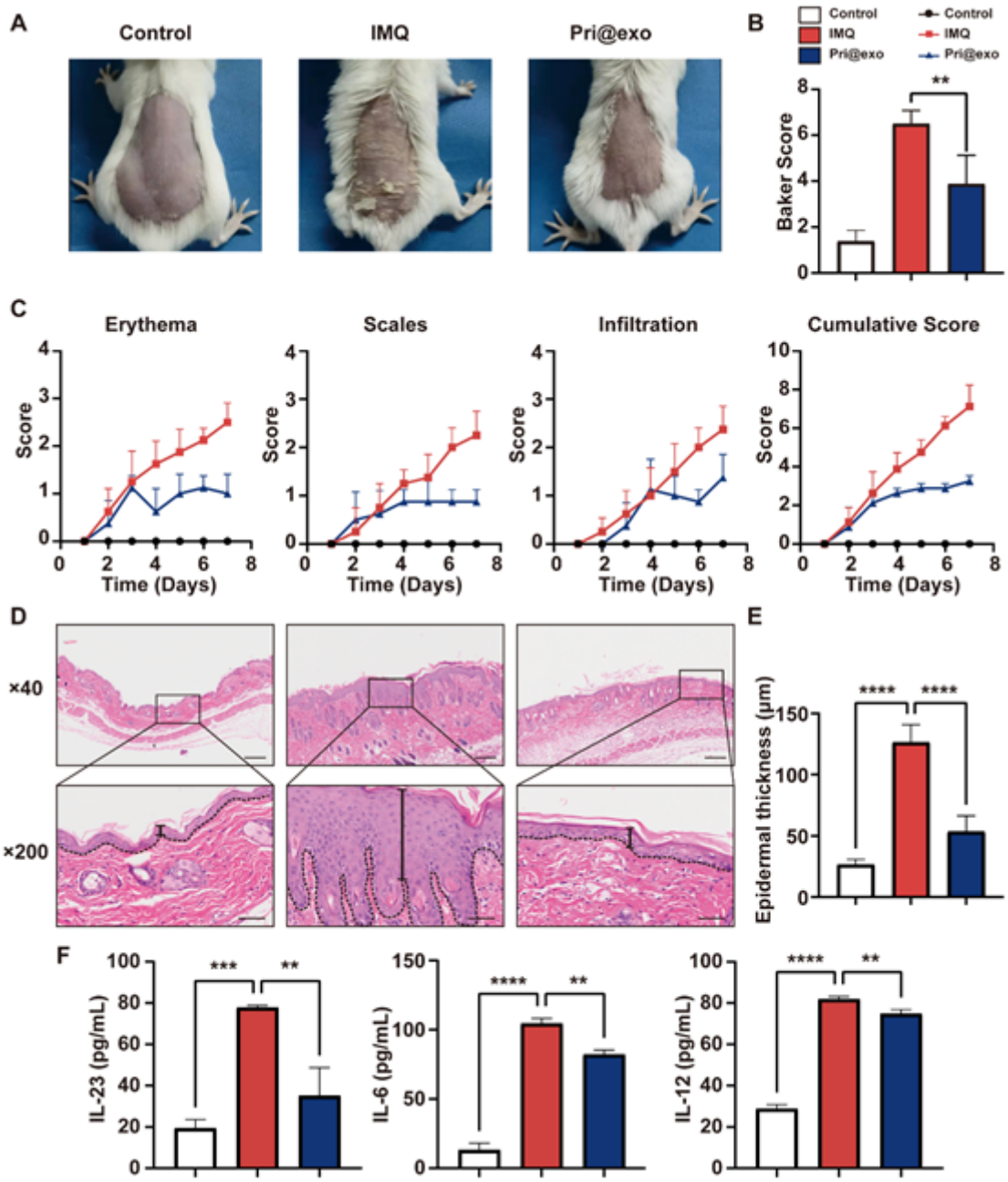

Figure 5

Pri@exo improves IMQ-induced psoriasis *in vivo*. (A) Representative back skin images from mice treated with various formulations. (B) H&E staining of the skin tissue sections from the mice after the specified treatments on day 7 (magnification, ×40 and ×200; scale bars, 200 and 50 μm, respectively). (C) A quantitative assessment of H&E staining was performed using Baker score. (D) Epidermal back skin thickness was measured microscopically. (E) Psoriasis area and severity index (PASI) scores were measured every day for seven days. (F) Expression levels of secreted pro-inflammatory cytokines, interleukin (IL)-23, IL-12, and IL-6, in plasma were determined by ELISA. The data are expressed as mean ± SD (n = 3 per group). **p < 0.01, ***p < 0.01, ****p < 0.001, ns, no significance.

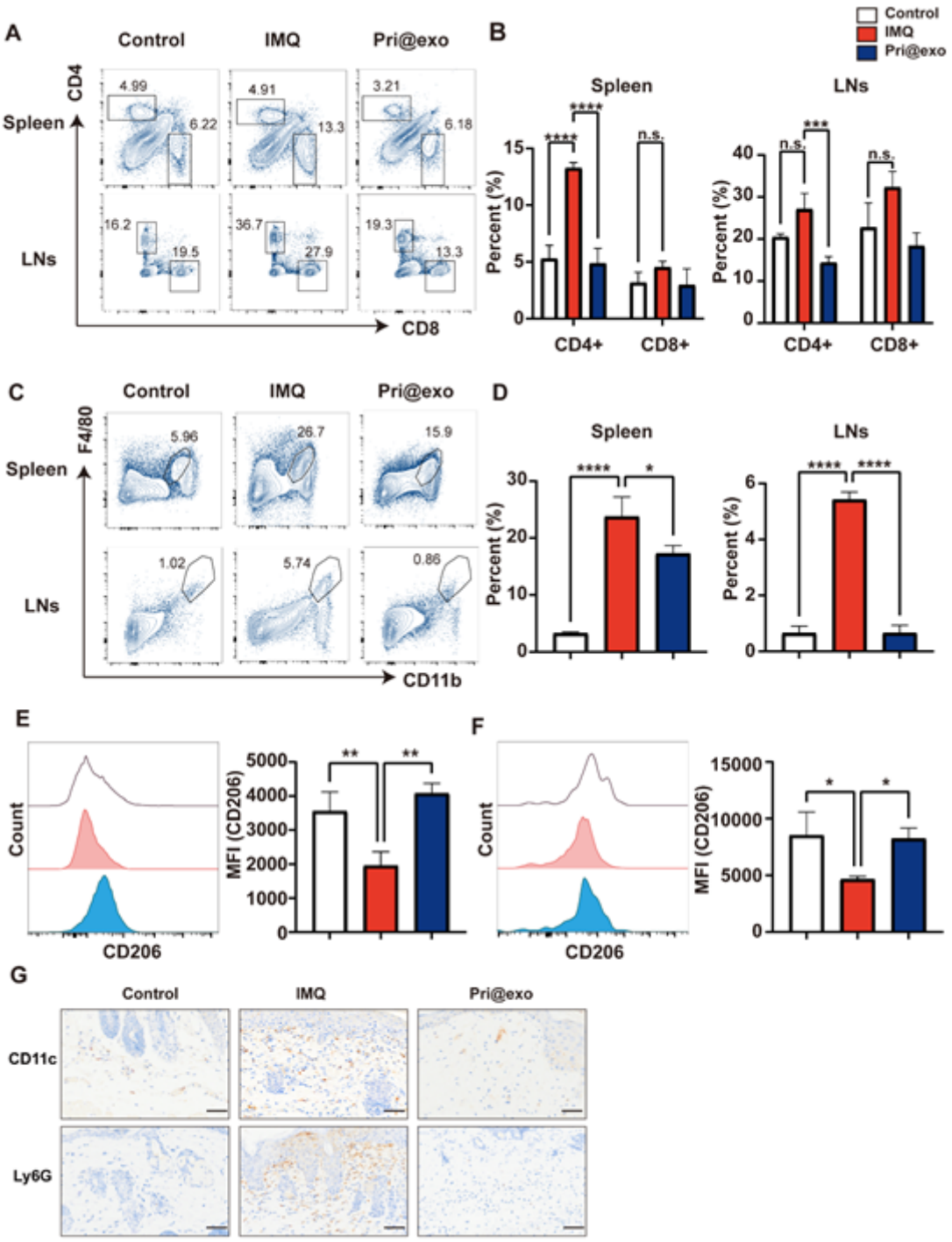

Figure 6

Pri@exo alters the percentages of immune cells in the spleens, lymphoid nodes (LNs), and skin by improving IMQ-induced psoriasis-like inflammation. (A) Flow cytometric analysis of $CD4^+$ T cells and $CD8^+$ T cells in spleens and LNs. (B) Quantitatively analysis of $CD4^+$ T cells and $CD8^+$ T cells in spleen and LNs. (C) Flow cytometric analysis of macrophages ($CD11b^+F4/80^{hi}$) in the spleens and LNs. (D) Quantitative analysis of macrophages in spleen and LNs. (E) Representative flow cytometry histograms (right) and quantitative analysis (left) of CD206 expression in macrophages in spleens. (F) Representative flow cytometry histograms (right) and quantitative analysis (left) of CD206 expression in

macrophages in LNs. (G) Representative immunohistochemistry images show expression staining of Ly6G and CD11c, which are the biomarker of neutrophils and dendritic cells, respectively, in skin tissues of mice. Scale bar, 50 μm. The data are expressed as mean ± SD (n = 3 per group). *p < 0.05, **p < 0.01, ***p < 0.01, ****p < 0.001, n.s., no significance

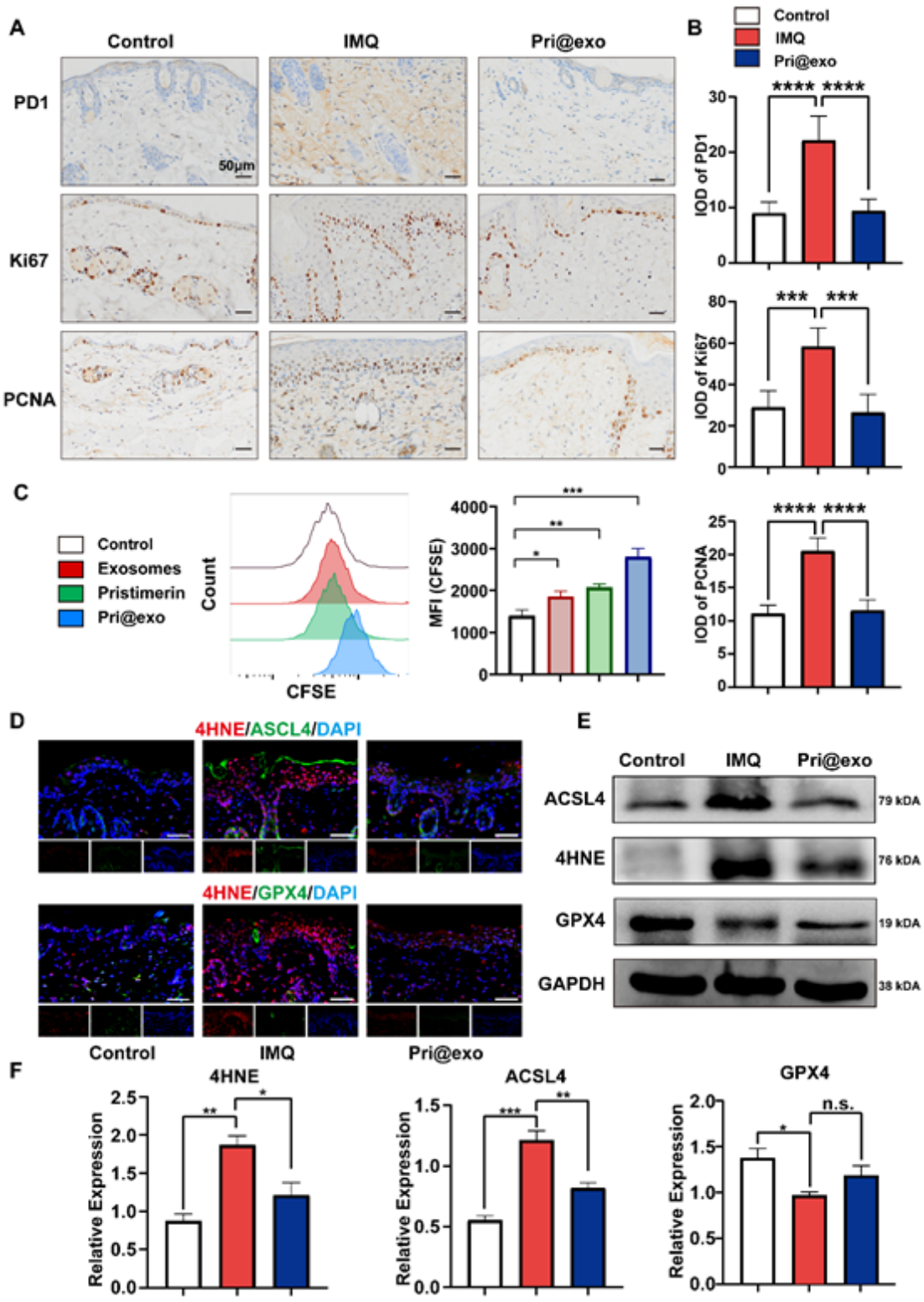

Figure 7

Pri@exo inhibits the proliferation of keratinocytes in psoriasis through ferroptosis. (A) Representative immunohistochemistry images illustrate the expression staining of PD-1, Ki67, and PCNA, in skin tissues of mice. (B) The quantification of PD1, Ki67, and PCNA (n = 5). (C) Representative flow cytometry histograms (left) and quantitative analysis (right) of CFSE in HaCaT cells. (D) Skin from a mouse treated with or without IMQ used for IF staining with antibodies against glutathione peroxidase 4 (GPX4) or Acyl-CoA synthetase long-chain family member 4 (ACSL4) (green) plus 4-hydroxynonenal (4HNE) (red). (E and F) Western blot analysis for ACSL4, 4HNE, GPX4, and GAPDH in the skin tissues from different groups (E) and the quantitative results of Western blotting (n = 3) (F). The data are expressed as mean ± SD. *p < 0.05, **p < 0.01, ***p < 0.01, n.s., no significance.

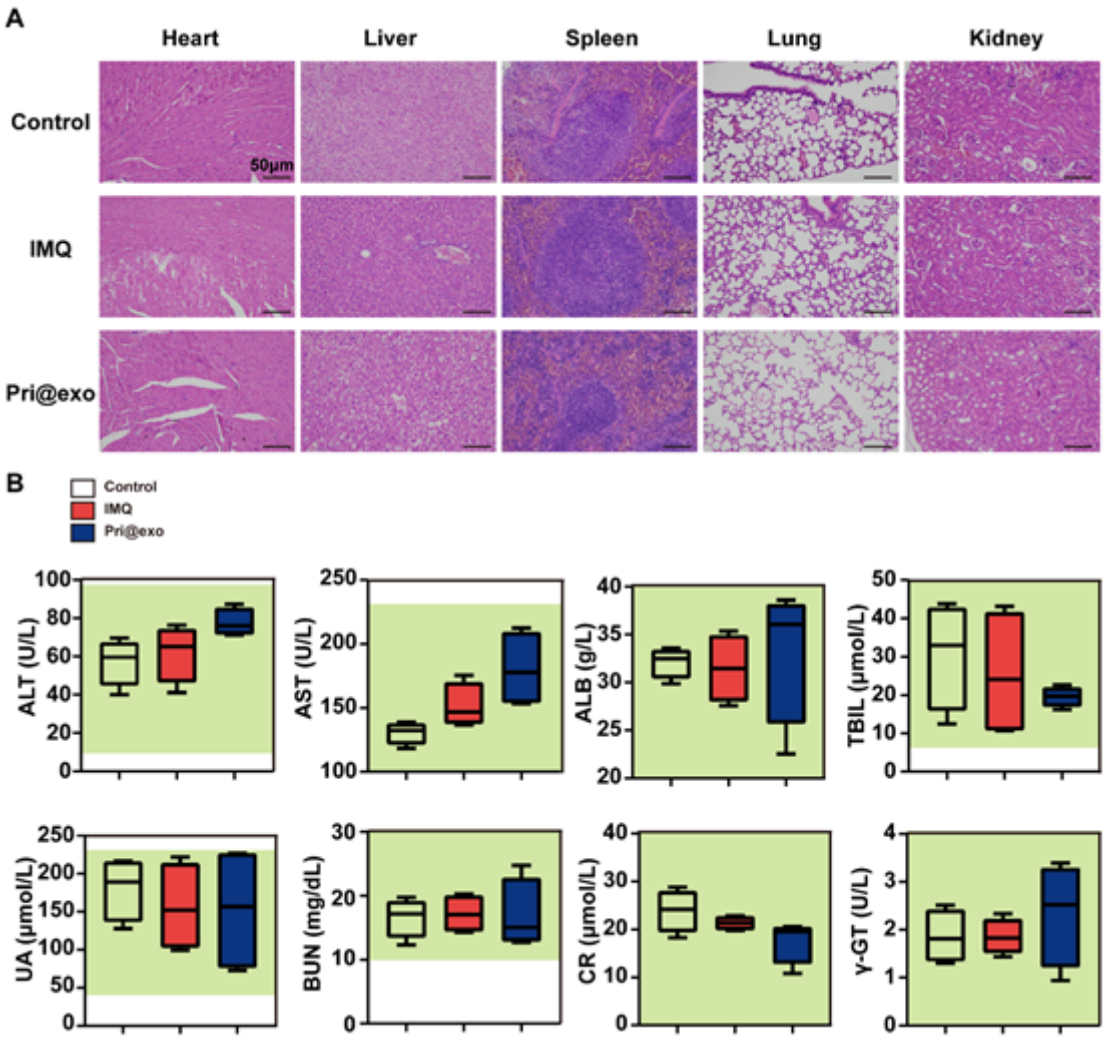

Figure 8

Biosafety of Pri@exo *in vivo*. (A) H&E-stained slice images of major organs (heart, liver, spleen, lung, and kidney) of three diverse treatment types (Control, IMQ, and Pri@exo) for IMQ-induced psoriasis. Scale bar, 50 μm. (B) Hematological analysis of mice from three diverse treatment types. Light green areas depict the normal range of different biosafety indicators. The data are expressed as mean ± SD (n = 4 per group).

Supplementary Files

This is a list of supplementary files associated with this preprint. Click to download.

- supplementaryinformation.docx
- graphabstract.tif